

Assessing the PAHAP potential with application to the exfoliation energy of graphite

Tim S. Totton¹, Alston J. Misquitta², Markus Kraft¹

released: 22 August 2011

¹ Department of Chemical Engineering
and Biotechnology
University of Cambridge
New Museums Site
Pembroke Street
Cambridge, CB2 3RA
United Kingdom
E-mail: mk306@cam.ac.uk

² Department of Physics
Cavendish Laboratory
University of Cambridge
J J Thomson Avenue
Cambridge, CB3 0HE
United Kingdom

Preprint No. 107



Keywords: PAH, anisotropic potential, PAHAP

Edited by

Computational Modelling Group
Department of Chemical Engineering and Biotechnology
University of Cambridge
New Museums Site
Pembroke Street
Cambridge CB2 3RA
United Kingdom

Fax: + 44 (0)1223 334796

E-Mail: c4e@cam.ac.uk

World Wide Web: <http://como.ceb.cam.ac.uk/>



Abstract

In this work we assess a recently published anisotropic potential for polycyclic aromatic hydrocarbon (PAH) molecules (*J. Chem. Theory Comput.* **2010**, 6, 683-695). Comparison to recent high-level SAPT(DFT) results for coronene (C₂₄H₁₂) demonstrate the transferability of the potential whilst highlighting some limitations with simple point charge descriptions of the electrostatic interaction. The potential is also shown to reproduce second virial coefficients of benzene (C₆H₆) with high accuracy and this is enhanced by using a distributed multipole model for the electrostatic interaction. The graphene dimer interaction energy and the exfoliation energy of graphite have been estimated by extrapolation of PAH interaction energies. The contribution of non-local fluctuations in the π electron density in graphite have also been estimated which increases the exfoliation energy by 3.0 meV atom⁻¹ to 47.6 meV atom⁻¹ which compares well to recent theoretical and experimental results.

Contents

1	Introduction	3
2	Numerical details	6
3	Assessment of the PAHAP potential	6
3.1	Comparing the PAHAP potential to SAPT(DFT) results for the coronene dimer	6
3.2	Calculation of the second virial coefficients of benzene	7
3.3	Binding energy of the graphene dimer	11
3.4	Exfoliation energy of graphite	13
3.4.1	π -electron contribution to the dispersion	14
4	Conclusions	16
	References	19

1 Introduction

Polycyclic aromatic hydrocarbon (PAH) molecules are an important class of molecules in the chemistry of hydrocarbon combustion. These molecules are found in a wide distribution of sizes in sooting flames [15–17, 25, 65, 85]. The examination of the resulting soot particles using high resolution TEM images reveals layered graphitic structures [11, 34, 82] and has led to the conclusion that clustering of PAH molecules is responsible for soot particle nucleation [27, 77, 92]. These findings have led to the development of predictive models to describe soot particle evolution in flame environments, such as engines [8, 9, 56, 66], but there remain many unanswered questions concerning the precise mechanisms of the nucleation and growth processes.

In order to access the structure and composition of nascent soot particles it is necessary to understand the interactions of PAH clusters at a molecular level. At present the most accurate means of doing this in a computationally feasible manner is by using atomistic intermolecular potentials. There have been many such potentials proposed in the literature, and they are often designed to be widely transferable between large classes of organic molecules [2, 6, 12, 35–37, 81, 86–88, 90], and are typically simple in form, treating all atom–atom interactions as isotropic. Often these potentials are augmented with a simple point charge model to account for the electrostatic interaction explicitly.

In the crystallographic community, intermolecular potentials have been developed for many years, notably by Williams [71, 86, 87] who used crystallographic data and heats of sublimation of organic molecules to parameterise Buckingham potentials with an additional point charge term. These potentials have been widely used in organic crystal structure prediction [3, 14, 42, 58, 63, 95] and on work with molecular clusters [20, 75]. The 1967 Williams version (W67) has been used in the context of PAH interactions by Miller [28] whilst the 1977 version (W77) has been fitted to a ‘Lennard-Jones plus point charges’ form [81] (termed the LJ potential) which has proved popular due to its computational efficiency [28, 67, 77].

The most recent of Williams’ potentials, the W99 potential [87], was originally derived from crystallographic data for hydrocarbon molecules but has since been extended to oxyhydrocarbon molecules [88] and nitrogen-containing molecules [89] to yield a model with 13 different atomic classes. For PAH molecules only the C(3) and H(1) classes are considered resulting in a PAH interaction potential with just 6 parameters as well as atomic point charges. In the crystallographic community Williams’ potentials have become benchmarks [62], and in a recent work we have shown that the W99 potential gives excellent agreement with high level quantum chemistry results for small stacked PAH dimers [78]. This agreement is due largely to the stacked dimers representing the lowest energy conformations which correspond to the crystal structures used to parameterise the potential. However, we also demonstrated that such potentials which use an isotropic atom-atom description of the intermolecular interaction cannot accurately model PAH interactions throughout conformational space. Consequently, if PAH interactions are to be accurately modelled in situations where non-stacked conformations are expected, *e.g.* in larger molecular clusters, a more complex atom-atom description is needed.

Until relatively recently, the paucity of experimental data and the computational limita-

tions of high-level quantum chemistry methods has precluded the development of complex atom-atom potentials. The development of new computational quantum chemistry methods which combine high accuracy with computational efficiency has enabled the development of a new class of specific, high-accuracy intermolecular potentials. In particular, the development of symmetry-adapted perturbation theory based on Kohn-Sham density functional theory orbitals (SAPT(DFT)) [29–32, 48–51] has led to a spate of new potentials, in part due to its high accuracy and computational efficiency. Equally importantly, however, is the feature of perturbation theory that allows us to naturally partition the total interaction energy into physical contributions: the exchange-repulsion, dispersion, polarisation and electrostatic interactions. This has enabled the parameterisation of potentials capable of modelling important details of intermolecular interactions such as atomic shape anisotropy, anisotropic polarizabilities and higher order dispersion contributions [13, 53, 55, 61, 63, 78, 80]. In particular, this approach was successfully used in a recent blind test of organic crystal structure prediction [53].

Podeszwa *et al.* [61] have used this methodology to develop an accurate intermolecular potential for benzene using SAPT(DFT) interaction energies. The form of this potential is a generalisation of the Buckingham potential, containing an exponential component multiplied by a quadratic term and a more detailed dispersion model including C_6 , C_8 and C_{10} terms. A point charge electrostatic term was also included and this along with the dispersion terms were multiplied by damping functions to attenuate the divergence at short intermolecular separations. In addition to the usual atomic sites this potential contained 13 off-atomic sites, resulting in a fit with a total of 92 parameters. The extra sites were required to account for the shape-anisotropy of the atomic sites in benzene. However, the large number of sites and parameters mean the potential is not obviously transferable to larger PAH molecules, and thus while it acts as a benchmark in terms of accuracy for benzene, it is not suitable for the study of the potential energy surface (PES) of PAH clusters.

In recent work [78] we developed a transferable, anisotropic, atomistic potential to describe the interactions of PAH molecules. This anisotropic potential was based on the methodology developed and successfully tested by Misquitta *et al.* [53] using a data set that included a large number of conformations of the benzene dimer and additionally dimers of larger PAH molecules (naphthalene, anthracene and pyrene [60]). The PAH anisotropic potential (PAHAP) was designed to be simple enough to maintain transferability amongst planar pericondensed PAH molecules, while accurately reproducing the interactions of these molecules for a large number of randomly chosen conformations. The potential was limited to three types of atom-atom interactions: carbon–carbon, carbon–hydrogen and hydrogen–hydrogen. Each of these atom-atom terms is dependent on the separation, R_{ab} , and relative orientation, Ω_{ab} , with a functional form given by

$$U_{ab} = \underbrace{G \exp \left[-\alpha_{ab} \left(R_{ab} - \rho_{ab}(\Omega_{ab}) \right) \right]}_{\text{short-range}} \underbrace{- f_6(R_{ab}) \frac{C_{6,\text{iso}}}{R_{ab}^6} + E_{\text{elst}}(\text{model})}_{\text{long-range}}. \quad (1)$$

The first term is a Born–Mayer term describing short-range interactions, the second is an isotropic, damped dispersion term, and the third term is an appropriate electrostatic model, which for simplicity we chose to be based on atom-centred point charges calculated using the Merz-Singh-Kollman scheme [69].

This form of the potential remedies two of the major deficiencies of traditional ‘exp-6’ potentials. Firstly, the short-range term now includes a shape-function, ρ_{ab} , which models the anisotropy of the interacting sites through a dependence on the relative orientation of the two sites:

$$\rho_{ab}(\Omega_{ab}) = \rho^a(\theta_a) + \rho^b(\theta_b), \quad (2)$$

where

$$\rho^a(\theta_a) = \rho_{00}^a + \rho_{10}^a \cos \theta_a + \frac{1}{2} \rho_{20}^a (3 \cos^2 \theta_a - 1) \quad (3)$$

and similarly for $\rho^b(\theta_b)$. Here the angle θ_a defines the angle between the site–site vector from a to b and the z -axis in the local axis system of site a . Since the anisotropy is included via shape-functions rather than additional sites, the resulting atom–atom potential is more clearly transferable to other PAH molecules.

Secondly, the singularity in the dispersion term is removed by a Tang–Toennies damping function [76], $f_6(R_{ab})$ for which the parameter β is calculated from the vertical ionisation potential of benzene I according to $\beta = 2(2I)^{1/2}$ [46],

$$f_n(R_{ab}) = 1 - \exp(-\beta R_{ab}) \sum_{k=0}^n \frac{(\beta R_{ab})^k}{k!}. \quad (4)$$

The resulting potential has a total of 12 parameters for the short-range and dispersion terms as well as the atom-centred point charges used in the electrostatic interaction.

SAPT(DFT) contributions up to second-order were used to fit the short-range term which included first-order exchange and penetration energies and second-order exchange-dispersion and exchange-induction energies. The isotropic C_6 dispersion model was calculated directly using the Williams-Stone-Misquitta method [45–47, 52, 91] and, due to a strong linear correlation found between the model energies and the SAPT(DFT) dispersion energies, a simple scaling factor was introduced to match SAPT(DFT) energies [46].

The PAHAP potential has been carefully parameterised using very accurate *ab initio* data from SAPT(DFT) and the WSM method, however two important short-comings remain: (1) The potential could not be considered transferable because a new set of point charges were needed for every type of PAH molecule, and (2) the potential was never validated against data not used in the fitting process.

We have remedied the first deficiency in a recent paper [79] by developing an electrostatic model for PAH molecules based on a transferable set of atom-centred quadrupole moments and point charges. In this paper we address the second deficiency by independent assessment of the potential against experimental data and very recent *ab initio* data. Firstly, we compare PAHAP and other potentials against recent high-level SAPT(DFT) calculations of coronene ($C_{24}H_{12}$) interactions. We then compare the potential with others against experimental data in the form of second virial coefficients of benzene. Finally, we use PAHAP to estimate the interaction energy of the graphene dimer and the exfoliation energy of graphite and compare results against experiment and recent high-level quantum calculations.

2 Numerical details

The geometries of all the molecules used in this work were optimised using density functional theory (DFT) with the B3LYP functional and the 6-31G* basis set. DFT calculations were also used to calculate electrostatic-potential-fitted (ESP) point charges for the electrostatic term using the Merz-Singh-Kollman scheme [69] with the PBE0 [1, 57] functional based on the optimised atomic coordinates. The basis set used for calculating charges depended on PAH size. The aug-cc-pVTZ was used for molecules up to the size of coronene ($C_{24}H_{12}$) and for larger molecules the cc-pVTZ basis set was used due to numerical instabilities encountered with the augmented version. All DFT calculations were performed using the GAUSSIAN03 program [22].

For most of our calculations we have used ESP charges, but for some we have used a more detailed distributed multipole description with multipoles up to rank 4 (hexadecapole) on the carbon atoms and up to rank 1 (dipole) on the hydrogen atoms. These distributed multipoles were calculated using the GDMA program [72, 73] from densities obtained using the PBE0 functional. Where there is potential ambiguity we have explicitly stated the kind of electrostatic model used with the PAHAP potential.

All evaluations of the PAHAP potential and other literature potentials were performed using the ORIENT program [74]. The local atomic axes used for the PAHAP potential, along with the distributed multipoles for benzene and coronene in ORIENT format are given in the Supporting Information. Also given are the geometries and ESP point charges for all the PAH molecules.

3 Assessment of the PAHAP potential

3.1 Comparing the PAHAP potential to SAPT(DFT) results for the coronene dimer

The PAHAP potential was originally fitted using SAPT(DFT) data for four small PAH molecules (benzene, naphthalene, anthracene and pyrene dimers), and while the potential was shown to model the interactions of these molecules very well, the lack of independent data to test the potential against weakened the claim of transferability. Recently SAPT(DFT) interaction energies for the coronene ($C_{24}H_{12}$) dimer have been calculated in a number of conformations [59] and provide the first opportunity to assess the transferability of PAHAP potential to larger PAH molecules.

The SAPT(DFT) calculations were performed by Podeszwa [59] using the aug-cc-pVDZ basis set [38] using the monomer-centred ‘plus’ (MC+) approach as used for the SAPT(DFT) calculations for the PAHAP potential. Figure 1 shows the four conformations for which potential curves were calculated by varying the interplanar distance. Figure 2 compares the PAHAP, W99 and LJ potentials with the SAPT(DFT) results. With one exception, which we will come to later, these potentials were all used with an ESP point-charge electrostatic model.

Three of the four conformations are very well matched by the PAHAP potential using the ESP charge model. For the fourth, sandwich conformation, the match is not as good; the well-depth is overestimated by around 10 kJ mol^{-1} ($\sim 15\%$ of the interaction energy), and the equilibrium separation is $\sim 0.1 \text{ \AA}$ smaller. This discrepancy is mainly due to the simplicity of the point-charge model. Also shown in figure 2 are interaction energies calculated using PAHAP with a more detailed distributed multipole electrostatic model. The agreement is clearly much better for the sandwich conformation, though this is accompanied with a slight degradation in accuracy at the other conformations. We expect some systematic error when using the distributed multipoles in place of ESP charges because the short-range terms in the PAHAP potential were obtained using electrostatic penetration energies calculated using ESP charges [78].

The improvement obtained with the distributed multipole model demonstrates the limitation of the simple point charge model. Figure 3 shows sections of the PES for the coronene dimer using the PAHAP potential with ESP charges and distributed multipoles. Here interaction energies are plotted with the monomers kept parallel to each other and moved around the xz plane. The twin minima in the potential wells show the two shifted graphite positions, and the smaller hump connecting the two corresponds to the sandwich position, identifying the conformation as a transition state between the two shifted graphite minima. The SAPT(DFT) results suggest that the energy of this saddle point is too low in the ESP case and that its location on the z axis should be further away from the repulsive wall.

The PES generated using distributed multipoles resolves the finer details of the energy landscape to a higher degree than the rather smoother PES generated using ESP charges. This is clearly demonstrated for sandwich conformation with a more accurately located saddle point. These results highlight the expected trade-off in accuracy when, in seeking to generate a simple transferable potential, a simple point charge electrostatic model is used. To maintain high accuracy in all conformations requires a more complex potential form, but the success of the PAHAP potential in prediction of the low-energy minima of the coronene dimer helps confirm its transferability to PAH interactions other than those from which it was originally parameterised.

Also shown in Figure 2 are interaction energy curves obtained with the W99 and LJ potentials. The W67 and W77 potentials are very similar to the LJ potential and are therefore not shown. As has been previously noted [78] the W99 potential is very accurate for these stacked conformations. However, we do not expect the W99 potential to fare as well in the non-stacked conformations where it has been shown to underestimate the binding of PAH molecules [78]. By contrast, the LJ potential (and W67 and W77 potentials) overestimates the well depths for all the conformations by at least 20 kJ mol^{-1} , and in the case of the sandwich conformation by more than 30 kJ mol^{-1} . This is a serious shortcoming and potentially undermines work based on these potentials.

3.2 Calculation of the second virial coefficients of benzene

The second (pressure) virial coefficient is a common source of experimental data directly related to the two-body interaction potential.

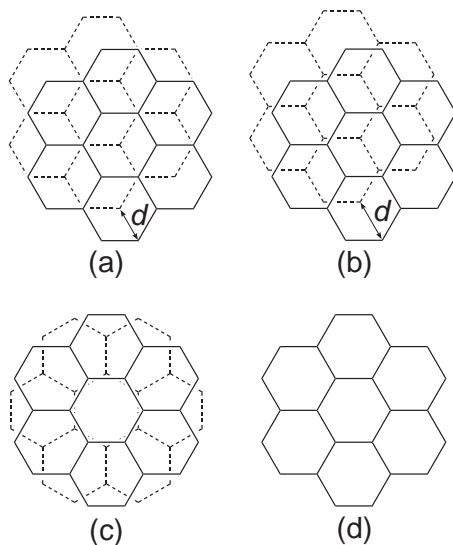


Figure 1: Structures of the coronene dimer: (a) graphite ($d = 1.43 \text{ \AA}$), (b) shifted graphite ($d = 1.65 \text{ \AA}$), (c) crossed (twisted sandwich), and (d) sandwich.

An expression for the second virial coefficient, $B(T)$, can be obtained from statistical mechanics which depends upon the pair potential only, even if many-body terms occur in the total energy. The variation of the second virial coefficient with temperature provides a way of examining the potential energy surface. At low temperatures the second virial coefficient is a measure of the volume of the potential well and at high temperatures it is a measure of the average size of the repulsive core, although both the repulsive and attractive parts of the potential surface contribute at each temperature. Since $B(T)$ is an integrated functional of the intermolecular potential, it is quite possible to obtain a good second virial coefficient with a poor potential. We shall see an example of this. We should therefore regard a good reproduction of $B(T)$ as a necessary rather than sufficient condition for an intermolecular potential.

In this work we have calculated the second virial coefficient of benzene for temperatures in the range 300-700 K using the ORIENT program. We have used the Gauss-Legendre integration scheme and have included the first-order quantum-correction [24, 33, 44], though the latter does not make a significant contribution owing to the relatively large mass and large moments of inertia of the benzene molecule; the effect being greatest at low temperature but still relatively small ($\sim 0.8\%$) at 200 K.

Figure 4 shows the second virial coefficients for the PAHAP potential with both ESP point charges and a full distributed multipole (DMA) electrostatic term. Also included are results obtained with the W67, W99 and LJ potentials and the benzene-specific potential from Podeszwa *et al.* We have taken the experimental data from Bich *et al.* [7], Wormald *et al.* [93] and Francis *et al.* [21] We see that the PAHAP(ESP) potential results in second virial coefficients that, while good at high temperatures, slightly underestimates the experimental values at low temperatures. This perhaps indicates that on average the potential slightly under-binds benzene. However, the PAHAP(DMA) potential is a clear improvement with excellent agreement with experiment across the temperature range. The Podeszwa *et al.* potential results in equally good virial coefficients.

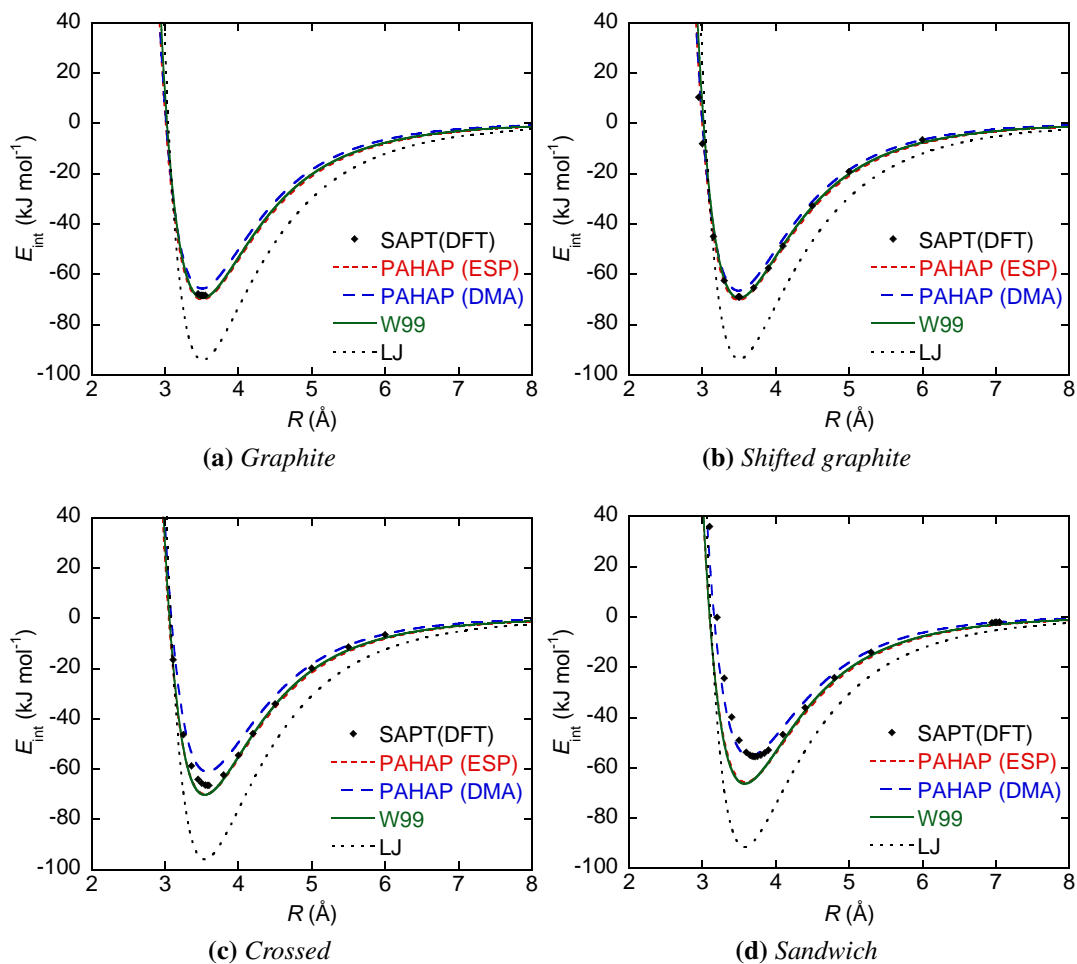


Figure 2: Comparison of potentials with SAPT(DFT) for stacked coronene dimer conformations. All potentials use the ESP point charge model except the PAHAP potential which is shown using both ESP charges and distributed multipoles (DMA). The Williams' 67 and 77 potentials (W67/W77) are not shown as they result in interaction energies very similar to those from the LJ potential.

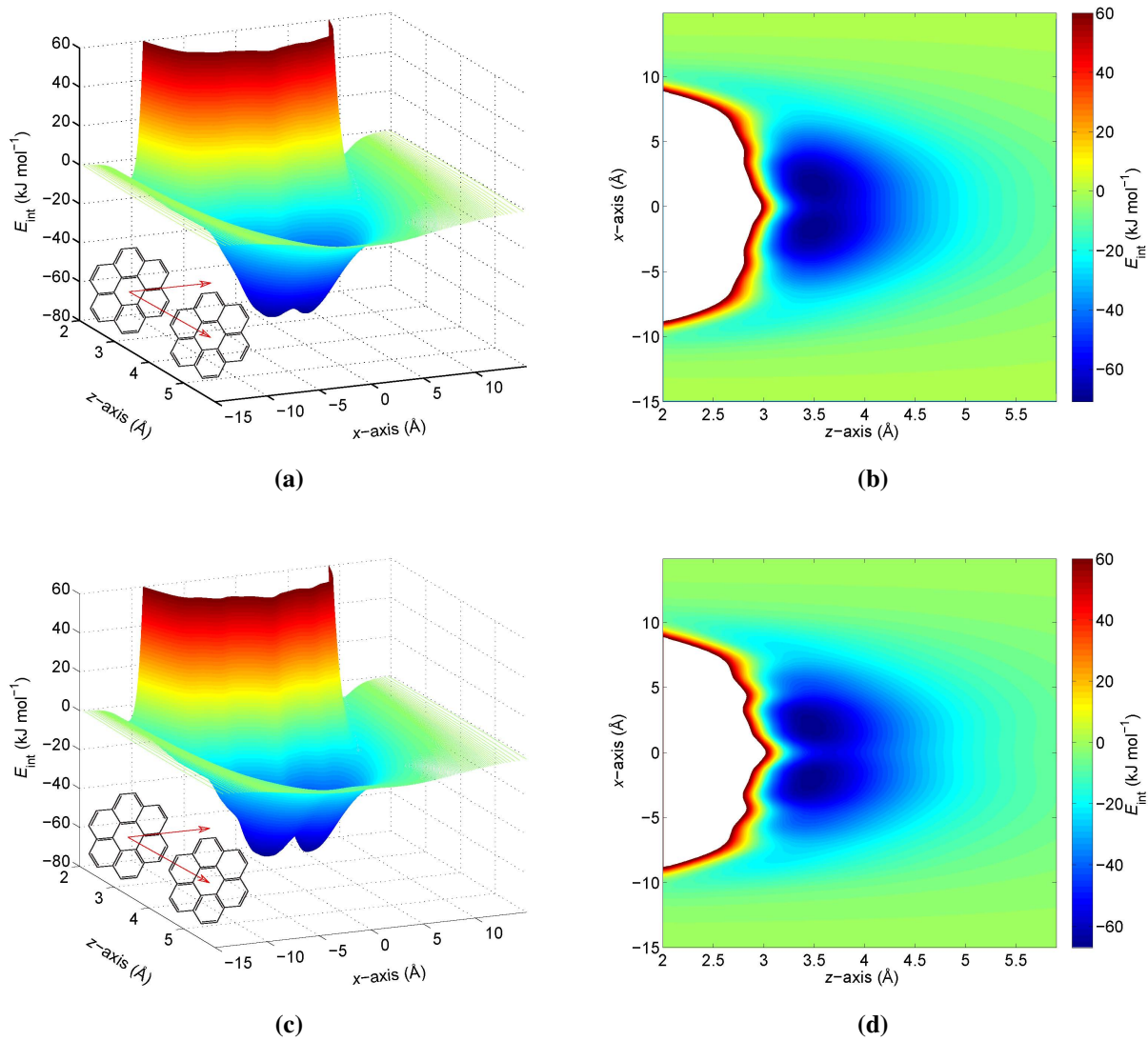


Figure 3: Potential energy surface for coronene dimer when one molecule is fixed and the other is kept parallel and moved in the xz plane calculate using the PAHAP potential with ESP charges, (a) and (b), and with distributed multipoles (DMA), (c) and (d).

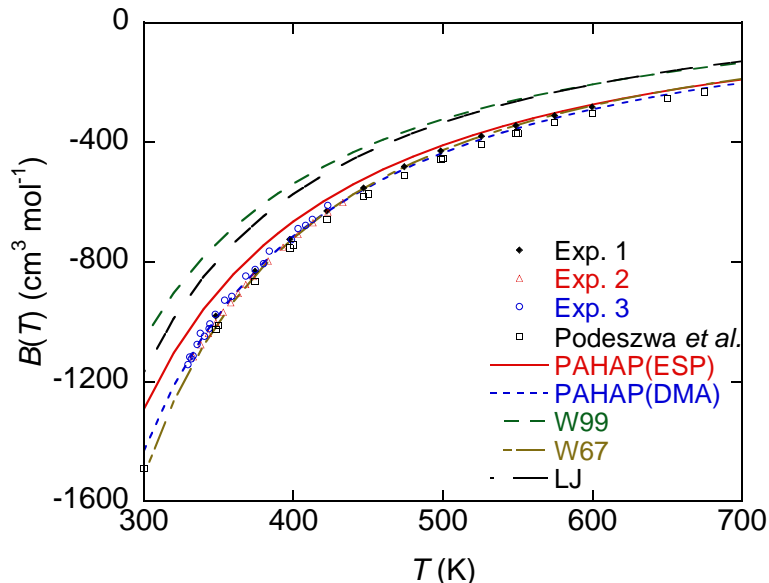


Figure 4: *Second virial coefficient of benzene. Experiment 1: ref. [7], Experiment 2: ref. [93], Experiment 3: ref. [21], Podeszwa potential: ref. [61], W99 potential: ref. [88], W67 potential: ref. [86], LJ potential: ref. [81]*

Although the W99 potential performs well for stacked conformations, we know [78] that this potential under-binds for other conformations, in particular the T-shaped conformation, and this seems to be reflected in systematic underestimation across the temperature range. Interestingly, while the W67 and LJ potentials appear to be almost identical for the coronene dimer, they result in quite different second virial coefficients for benzene. The W67 potential matches the experimental data almost perfectly whereas the LJ potential underestimates the data. However, as we have stated before, a good second virial coefficient does not imply an accurate potential. In the case of the W67 potential this is highlighted in the overestimation of the well depth for stacked conformations of the coronene dimer (section 3.1), a trend also seen for benzene, which suggests other areas of the PES must be underestimated to give an accurate average interaction.

3.3 Binding energy of the graphene dimer

The interaction energy of stacked homo-molecular PAH dimers (per number of monomer carbon atoms) increases with increased dimer mass, but tends towards an asymptote corresponding to the interaction energy of two infinite graphene sheets (Figure 6). This is an important limit from the theoretical viewpoint, but also because PAH molecules in soot, while not infinite in extent, can be very large, comprising hundreds of atoms [64].

An estimate of the interaction energy of two graphene sheets can be found by extrapolating the interaction energies for the stacked PAH dimers using a simple two-parameter model [26, 59]:

$$\frac{E_{\text{int}}(n_{\text{C}})}{n_{\text{C}}} = \frac{an_{\text{C}}}{b + n_{\text{C}}} \quad (5)$$

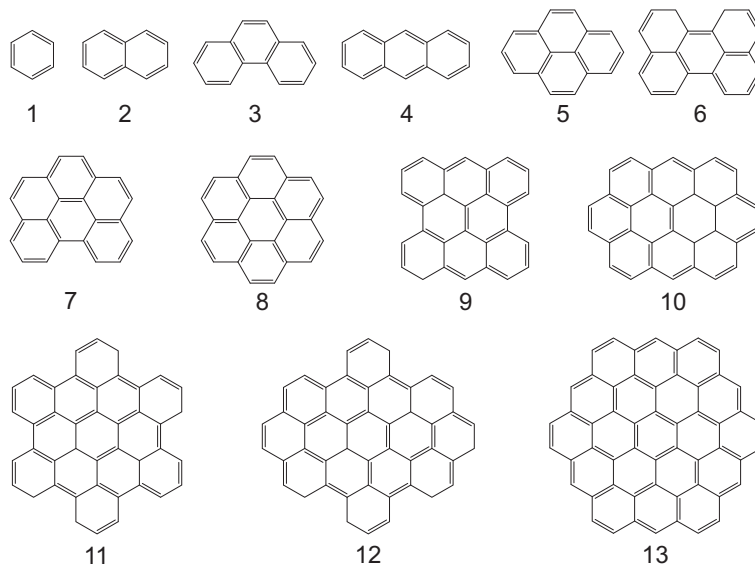


Figure 5: The pericondensed PAH molecules studied in this work: 1. Benzene (C_6H_6), 2. Naphthalene ($C_{10}H_8$), 3. Phenanthrene ($C_{14}H_{10}$), 4. Anthracene ($C_{14}H_{10}$), 5. Pyrene ($C_{16}H_{10}$), 6. Perylene ($C_{20}H_{12}$), 7. Benzo[*g,h,i*]perylene ($C_{22}H_{12}$), 8. Coronene ($C_{24}H_{12}$), 9. Bisanthene ($C_{28}H_{14}$), 10. Ovalene ($C_{32}H_{14}$), 11. Hexabenzocoronene ($C_{42}H_{18}$), 12. Octabenzocoronene ($C_{46}H_{18}$), 13. Circumcoronene ($C_{54}H_{18}$)

where n_C is the number of carbon atoms per monomer and a and b are fitted parameters. This satisfies the physical constraints of the system, being zero for $n_C = 0$ and asymptotically constant for large n_C . The interaction energy per carbon atom for the graphene dimer is given by the limit as $n_C \rightarrow \infty$, which is simply a .

Interaction energies for homomolecular PAH dimers were calculated for 13 different PAH molecules (Figure 5) using the GMIN program [83]. With this program, molecular cluster geometry is optimised using the ‘basin hopping’ method [10, 41, 77, 84] which combines local gradient-based minimisation with a Metropolis Monte Carlo scheme allowing different ‘basins’ on the PES to be located and ‘hopped’ between. This method provides an efficient scheme to sample the potential energy landscape.

We obtain an estimate for the interaction energy of the graphene dimer of $a = 3.94 \text{ kJ mol}^{-1}$ per carbon atom ($40.9 \text{ meV atom}^{-1}$) and $b = 7.59$, using interaction energies calculated with the PAHAP potential for dimers of PAH molecules shown in Figure 5. The rms deviation for the fit is 0.06 kJ mol^{-1} per carbon atom ($0.6 \text{ meV atom}^{-1}$). We excluded benzene from the fit to Eqn. 5 as the minimum energy conformation of the benzene dimer is not stacked (it is a tilted T-shaped structure[61]). This result is similar to that found by Podeszwa [59], who, using SAPT(DFT) calculations of interaction energies of three PAH dimers (anthracene, pyrene and coronene) together with the extrapolation method described above, obtained a graphene dimer interaction energy of $42.5 \text{ meV atom}^{-1}$.

There are, however, key differences in our approaches: we have used minimum energy dimer conformations while Podeszwa constrained the dimer to be in the graphite configuration and optimized interplanar separation only. By using SAPT(DFT) interaction

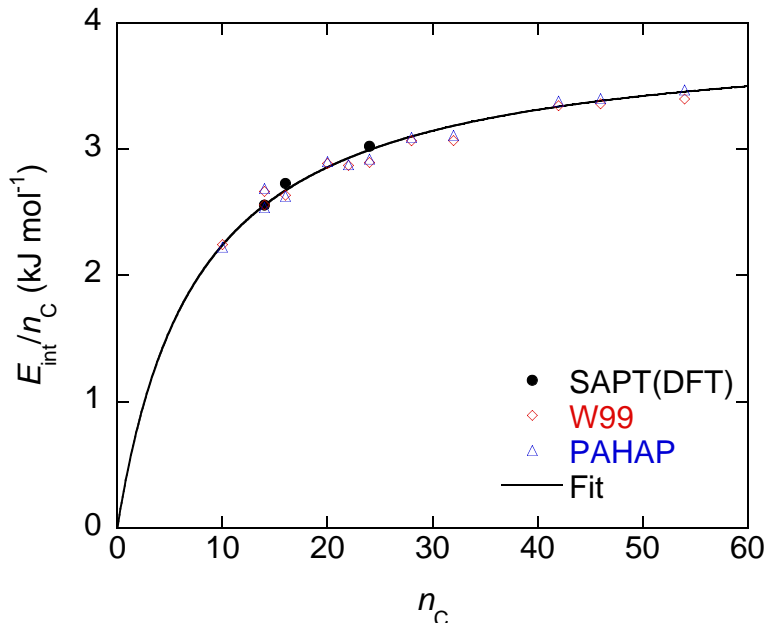


Figure 6: Interaction energies for PAH dimers using the PAHAP and W99 potentials. The SAPT(DFT) energies used in Ref. [59] are included for comparison. These energies were calculated using the full dimer-centered basis set plus mid-bonds (DC^+BS) approach and were used to estimate the interaction energy of graphene (Table 1). A fit of the PAHAP results using Eqn. 5 is shown with parameters $a = 3.94 \text{ kJ mol}^{-1}$ and $b = 7.59$.

energies with a 1-dimensional fit Podeszwa minimizes the errors due to fitting, but consequently, only a few small dimers can be used. This leads to an uncertainty in the extrapolation using Eqn. 5. This uncertainty is largely removed in our approach, as with a potential a much larger number of dimers can be sampled, thereby leading to a better control of extrapolation errors. The similarity of our results suggests that these differences are probably inconsequential. Our results also serve as a validation of the extrapolation formula (Eqn. 5).

3.4 Exfoliation energy of graphite

The exfoliation energy of graphite is the energy required for the uppermost graphene layer to be removed from the graphite surface. This is different from the interaction energy of two graphene sheets due to the interaction with graphene planes other than the nearest neighbour.

The exfoliation energy must be differentiated from the binding energy and cleaving energy: the former is the interaction energy per carbon in the graphite crystal and the latter is the energy released per carbon upon cleaving a graphite crystal into two along a graphene plane. Unfortunately, these energies are often undifferentiated in theoretical and experimental papers, but because the dominant interaction is between nearest layers, the differences in these three energies is expected to be small and is probably well within the

uncertainties in the experimental data.

Experimental values vary widely between the most recent value of $52 \pm 5 \text{ meV atom}^{-1}$ [94] measured from the thermal desorption of PAHs on graphite, and much lower older experimental results ($35_{-10}^{+15} \text{ meV atom}^{-1}$ [5], 43 meV atom^{-1} [23]. The latter result has been erroneously quoted as 21 meV atom^{-1} in some literature.). Table 1 compares the PAHAP values with a number of experimental and higher-level numerical estimations.

An estimate of the exfoliation energy for graphite can be gained using a similar method as used to estimate the graphene dimer interaction energy by using the attachment energy E_{attach} of a PAH to a small homomolecular stack which is defined as:

$$E_{\text{attach}} = E_{\text{int}}^k - E_{\text{int}}^{k-1}, \quad (6)$$

where E_{int}^k is the interaction energy for a homomolecular stack of k molecules. This implicitly includes the interaction of the top molecule with layers other than the nearest neighbour.

Interaction energies for homomolecular stacks were found using the GMIN program under constraints to ensure that only stacked configurations were obtained. The constraints were fairly weak and allowed molecules to arrange in the most energetically favourable way in the stack (not necessarily a *parallel* stack, though often, near-parallel stacks were obtained). This freedom meant that sometimes graphitic conformations were not found. These energies were then used to calculate asymptotic limits for each value of k (number of molecules in the stack), giving parameter a according to Eqn. 5 (see Figure 7). Energies for molecules smaller than pyrene were not included in the extrapolation as they tended not to form stable stacks. The value of a for $k = 2$ corresponds to the estimate of the graphene interaction energy described above. For $k > 2$ the value of a does not change by much, indicating that the interaction arises predominantly from two layers. An estimate of the exfoliation energy for graphite was obtained as the average of the results for $k > 2$, and was found to be $a = 44.6 \pm 0.4 \text{ meV atom}^{-1}$ with $b = 8.1 \pm 0.3$. Once again, this compares reasonably well with the work of Podeszwa [59] ($45.3 \text{ meV atom}^{-1}$), although our lower value suggests that the PAHAP potential may slightly underestimate well-depths in the stacked configuration.

3.4.1 π -electron contribution to the dispersion

Semi-classically, the van der Waals dispersion interaction may be interpreted as arising from the correlation between quantum mechanical density fluctuations in the interacting species. Implicit in this picture is the tacit assumption that these fluctuations are *local*, in the sense that they remain associated with the atom (in a molecule), from which we obtain the familiar $-\sum_{ab} C_6^{ab} R_{ab}^{-6}$ expression for the van der Waals dispersion energy (to leading order). This is the assumption made in the PAHAP potential. But recently it has been shown that for small, or zero gap, extended systems this assumption breaks down, or is at best incomplete, with a contribution to the van der Waals interaction arising from *non-local* density fluctuations [18, 54]. Within this picture, the van der Waals interaction in graphite has been shown to arise from two types of electron correlation [18]: a correlation between *local* density fluctuations in the sp^2 electrons and a correlation between *non-local* density fluctuations in the delocalized π electrons.

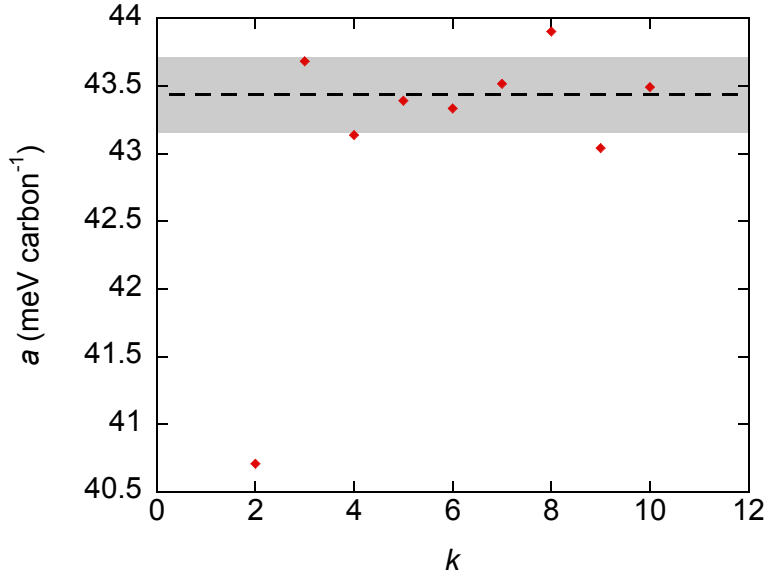


Figure 7: The asymptotic limit of the binding energy per carbon atom as estimates of the exfoliation energy of graphite. The dashed line indicates the average value excluding the result for $k = 2$ and the grey area indicates the standard deviation.

Our calculations of the binding energy of graphene and the exfoliation energy of graphite do not include the latter. First of all, this is because of the form of the van der Waals dispersion energy in the PAHAP potential, and secondly because we have attempted to approach the graphene limit by extrapolating from finite-sized PAHs. Dobson *et al.* [18] have shown that the non-local fluctuations arising from the π electron density in graphite result in an effective $-c_3 D^{-3}$ contribution, where D is the interlayer separation. This has been confirmed recently by Lebegue *et al.* using the ACFDT-RPA method [40], who have also been able to isolate this contribution and have obtained $c_3 = 487.6 \text{ meV \AA}^3$ per unit cell (containing four atoms). Although this result was obtained for bulk graphite, we can use it to estimate the importance of the non-local fluctuations to the binding energy. We have done this using a stack of 10 circumcoronene molecules fixed in the graphite AB stacking configuration. As we see in Figure 8, the c_3 term contributes an additional $3.0 \text{ meV atom}^{-1}$ to the exfoliation energy. As noted by Lebegue *et al.*, the effect of this term is small, but it is in the right direction: with this term included our estimate of the exfoliation energy of $47.6 \text{ meV atom}^{-1}$ compares well with the binding energy computed by Lebegue *et al.* as well as the recent experimental binding energy result from Liu *et al.* [43].

The interlayer separation of graphite is difficult to estimate using finite systems, particularly if we do not enforce the graphitic structure. Variations are significant and an extrapolation to the graphite limit is apparently impossible. For the 10 circumcoronene stack described above, we obtain a minimum in the energy at an interlayer separation of 3.46 \AA . This is larger than the experimental value of 3.34 \AA [4] by 0.12 \AA . The c_3 term reduces the separation slightly to 3.44 \AA , leaving a residual discrepancy of 0.10 \AA (see Figure ??). There are a few possible reasons for this difference: circumcoronene may not be large enough to represent graphene and an extrapolation may be required. Podeszwa [59] has

Table 1: Binding energies for the graphene dimer and exfoliation and binding energies of graphite. Energies are given in meV atom^{-1} .

Method	$E_{\text{int}}(\text{graphene})$	$E_{\text{exf}}(\text{graphite})$	$E_{\text{int}}(\text{graphite})$	Note
PAHAP	40.9 ± 0.6	44.6 ± 0.4		Present work
SAPT(DFT)	42.5	45.3		ref. [59]; SAPT(DFT) interactions of small dimers
ACFDT-RPA			48	ref. [40]; Adiabatic-connection fluctuation-dissipation theorem in random phase approximation calculation of interlayer binding energy
QMC			56 ± 5	ref. [70]; Quantum Monte Carlo calculations of equilibrium interlayer binding energy
QMPFF	49.9	54.9		ref. [19]; Potential fitted to <i>ab initio</i> interaction energies of small dimers
vdW-DF			24	ref. [39]; van der Waals density functional theory
DFT-D		54		ref. [68]; Supermolecular DFT-D using DFT/CCSD(T) correction scheme
B97-D	66			ref. [26]; Supermolecular DFT-D using an empirical correction
Exp.		43		ref. [23]; energy of wetting at room temperature
Exp.			35^{+15}_{-10}	ref. [5]; measurements of cross-sections of deformed carbon nanotubes
Exp.		52 ± 5		ref. [94]; thermal desorption of PAHs on graphite
Exp.			44 ± 3	ref. [43]; Atomic force microscopy over graphite flakes

attempted such an extrapolation using much smaller PAH molecules and stacks and obtains a very similar interlayer separation. A more probable reason may be that the PAHAP potential has been fitted to energies and not geometries, or perhaps, as Podeszwa has suggested, the SAPT(DFT) interaction energies on which the PAHAP potential is based are not yet saturated with respect to basis set.

4 Conclusions

The PAHAP potential has been assessed by comparison against experiment and high-level *ab initio* data. In assessing the accuracy of the potential, firstly, comparison of the potential with high-level SAPT(DFT) calculations for the coronene dimer reveals very close matches for the three lowest-energy conformations sampled. This confirms the transferability of the potential to PAH molecules larger than the four molecules on which the potential was originally parameterised. With the simple ESP point charge electrostatic model the transitional ‘sandwich’ conformation well depth was overestimated by $\sim 15\%$. Using a more elaborate distributed multipole electrostatic model, this was reduced such that the well depth residual error became 0.2%. This highlights the need for more com-

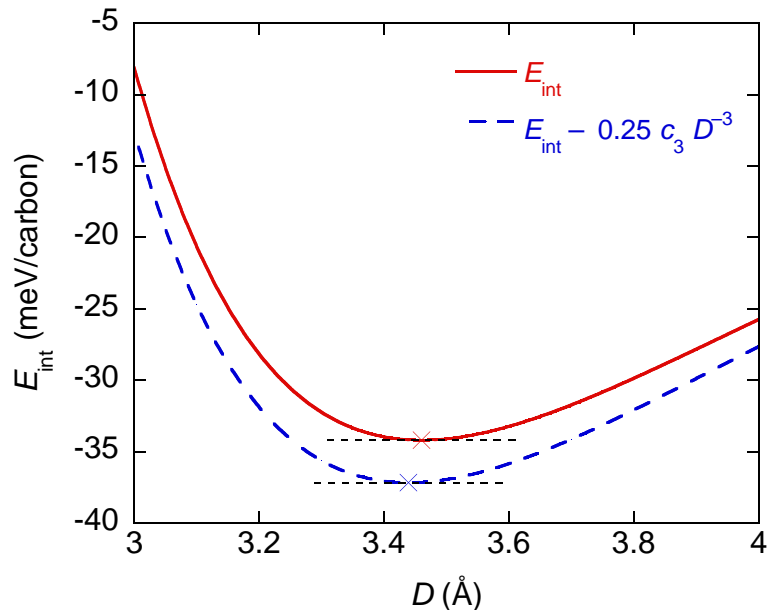


Figure 8: c_3 contribution to the interaction energy for a 10-layered circumcoronene stack (in the graphite AB configuration). We report the interaction energy per carbon with the PAHAP potential and additionally with the $-0.25c_3D^{-3}$ term calculated using data from Lebegue *et al.* [40]. The factor of 0.25 is used as the value of c_3 reported by Lebegue *et al.* is per unit cell (which contains four atoms).

plex descriptions of the electrostatic interaction if all conformations are to be accurately modelled.

Secondly, the second virial coefficients for benzene, calculated over a broad range of temperatures have been shown to reproduce experimental values. The residual errors at low temperatures are removed by replacing the ESP point charge electrostatic model with the distributed multipole model. These results have been shown to be significantly more accurate than those calculated with the empirical Williams '99 potential, which represents a benchmark transferable potential in the literature, and are comparable to results obtained using the benzene-specific potential derived by Podeszwa *et al.* [61].

Thirdly, by extrapolating interaction energies of homomolecular PAH stacks, estimates were obtained for the interaction energy of the graphene dimer ($40.9 \text{ meV atom}^{-1}$) and the exfoliation energy of graphite ($44.6 \text{ meV atom}^{-1}$). These results are very similar to those obtained by Podeszwa [59], but through our approach uncontrolled errors in the extrapolation are significantly reduced. The contribution of long wavelength, non-local fluctuations associated with the π -electron density in graphite have also been estimated using data from recent calculations by Lebegue *et al.* [40]. This increases the exfoliation energy to $47.6 \text{ meV atom}^{-1}$, bringing it into line with recent theoretical results by Lebegue *et al.* and experimental results by Liu *et al.* [43].

These results combine to highlight the transferability of the PAHAP potential whilst maintaining high accuracy. The potential will form the basis of further studies into the nucleation of PAH clusters in high temperature environments, corresponding to the conditions seen for soot formation in flames. For this application quantitatively accurate descriptions

of the underlying potential energy surfaces are required to determine the size of nucleating species and the process kinetics, which will depend exponentially on the binding energies.

Acknowledgements

We thank Dr Roger Cracknell for useful discussions. T.S.T. gratefully acknowledges financial support from the EPSRC, Shell Research Ltd. and Churchill College, Cambridge.

Supporting Information

Monomer coordinates with partial atomic point charges for the 13 PAH molecules used in this work are provided. Axes files which define the local axis system used for each molecule are also provided for use with the ORIENT program [74]. Additionally the distributed multipoles up to rank 4 for the carbon atoms and rank 1 for the hydrogen atoms are provided for the benzene and coronene molecules.

References

- [1] C. Adamo and V. Barone. Toward reliable density functional methods without adjustable parameters: The PBE0 model. *The Journal of Chemical Physics*, 110(13): 6158–6170, 1999. doi:10.1063/1.478522.
- [2] N. L. Allinger, Y. H. Yuh, and J. H. Lii. Molecular mechanics. The MM3 force field for hydrocarbons. 1. *Journal of the American Chemical Society*, 111(23):8551–8566, 1989. doi:10.1021/ja00205a001.
- [3] Y. A. Arnautova, A. Jagielska, J. Pillardy, and H. A. Scheraga. Derivation of a new force field for crystal-structure prediction using global optimization: Nonbonded potential parameters for hydrocarbons and alcohols. *The Journal of Physical Chemistry B*, 107(29):7143–7154, 2003. doi:10.1021/jp0301498.
- [4] Y. Baskin and L. Meyer. Lattice constants of graphite at low temperatures. *Physical Review*, 100(2):544, 1955. doi:10.1103/PhysRev.100.544.
- [5] L. X. Benedict, N. G. Chopra, M. L. Cohen, A. Zettl, S. G. Louie, and V. H. Crespi. Microscopic determination of the interlayer binding energy in graphite. *Chemical Physics Letters*, 286(5-6):490–496, 1998. doi:10.1016/S0009-2614(97)01466-8.
- [6] T. Beyer and S. L. Price. Dimer or Catemer? Low-Energy Crystal Packings for Small Carboxylic Acids. *The Journal of Physical Chemistry B*, 104(12):2647–2655, 2000. doi:10.1021/jp9941413.
- [7] E. Bich, H. Hendl, T. Lober, and J. Millat. Quasi-isochoric $p\rho T$ measurements, 2nd virial coefficient and vapor pressure of benzene. *Fluid Phase Equilibria*, 76:199–211, 2004. doi:10.1016/0378-3812(92)85088-P.
- [8] M. S. Celnik, A. Raj, R. H. West, R. I. A. Patterson, and M. Kraft. An aromatic site description of soot particles. *Combustion and Flame*, 155(1-2):161–180, 2008. doi:10.1016/j.combustflame.2008.04.011.
- [9] M. S. Celnik, M. Sander, A. Raj, R. H. West, and M. Kraft. Modelling soot formation in a premixed flame using an aromatic-site soot model and an improved oxidation rate. *Proceedings of the Combustion Institute*, 32(1):639–646, 2009. doi:10.1016/j.proci.2008.06.062.
- [10] D. Chakrabarti and D. J. Wales. Simulations of rigid bodies in an angle-axis framework. *Physical Chemistry Chemical Physics*, 11(12):1970–1976, 2009. doi:10.1039/b818054g.
- [11] H. X. Chen and R. A. Dobbins. Crystallogenesi s of particles formed in hydrocarbon combustion. *Combustion Science and Technology*, 159(1):109–128, 2000. doi:10.1080/00102200008935779.

- [12] D. S. Coombes, S. L. Price, D. J. Willock, and M. Leslie. Role of electrostatic interactions in determining the crystal structures of polar organic molecules. A distributed multipole study. *The Journal of Physical Chemistry*, 100(18):7352–7360, 1996. doi:10.1021/jp960333b.
- [13] G. M. Day and S. L. Price. A nonempirical anisotropic atom–atom model potential for chlorobenzene crystals. *Journal of the American Chemical Society*, 125(52):16434–16443, 2003. doi:10.1021/ja0383625.
- [14] G. M. Day, T. G. Cooper, A. J. C. Cabeza, K. Hejczyk, H. L. Ammon, S. X. M. Boerrigter, J. Tan, R. G. D. Valle, E. Venuti, J. Jose, S. R. Gadre, G. R. Desiraju, T. S. Thakur, B. P. van Eijck, J. C. Facelli, V. E. Bazterra, M. B. Ferraro, A. Gavezzotti, D. W. M. Hofmann, M. Neumann, F. J. J. Leusen, J. K. S. L. Price, A. J. Misquitta, P. G. Karamertzanis, G. Welch, H. A. Scheraga, Y. A. Arnautova, M. U. Schmidt, J. van de Streek, A. Wolf, and B. Schweizer. Significant progress in predicting the crystal structures of small organic molecules - a report on the fourth blind test. *Acta Crystallographica Section B*, 65:107–125, 2009.
- [15] R. A. Dobbins, R. A. Fletcher, and W. Lu. Laser microprobe analysis of soot precursor particles and carbonaceous soot. *Combustion and Flame*, 100(1-2):301–309, 1995. doi:10.1016/0010-2180(94)00047-V.
- [16] R. A. Dobbins, R. A. Fletcher, and H. C. Chang. The evolution of soot precursor particles in a diffusion flame. *Combustion and Flame*, 115(3):285–298, 1998. ISSN 0010-2180. doi:10.1016/S0010-2180(98)00010-8.
- [17] R. A. Dobbins, R. A. Fletcher, B. A. Benner Jr., and S. Hoefft. Polycyclic aromatic hydrocarbons in flames, in diesel fuels, and in diesel emissions. *Combustion and Flame*, 144(4):773–781, 2006. doi:10.1016/j.combustflame.2005.09.008.
- [18] J. F. Dobson, A. White, and A. Rubio. Asymptotics of the dispersion interaction: Analytic benchmarks for van der waals energy functionals. *Physical Review Letters*, 96(7):073201, 2006. doi:10.1103/PhysRevLett.96.073201.
- [19] A. G. Donchev. Ab initio quantum force field for simulations of nanostructures. *Physical Review B*, 74(23):235401, 2006. doi:10.1103/PhysRevB.74.235401.
- [20] D. C. Easter. Identification of a new c_3 structure and evidence for the co-existence of two $(\text{Benzene})_{13}$ cluster isomers in free jet expansions: A monte carlo study. *The Journal of Physical Chemistry A*, 107(39):7733–7742, 2003. doi:10.1021/jp035694n.
- [21] P. G. Francis, M. L. McGlashan, and C. J. Wormald. A vapour-flow calorimeter fitted with an adjustable throttle. The isothermal joule-thomson coefficient of benzene. The temperature-dependence of the second virial coefficient of benzene. *The Journal of Chemical Thermodynamics*, 1(5):441–458, 1969. doi:10.1016/0021-9614(69)90003-2.

- [22] M. J. Frisch, G. W. Trucks, H. B. Schlegel, G. E. Scuseria, M. A. Robb, J. R. Cheeseman, J. A. Montgomery, Jr., T. Vreven, K. N. Kudin, J. C. Burant, J. M. Millam, S. S. Iyengar, J. Tomasi, V. Barone, B. Mennucci, M. Cossi, G. Scalmani, N. Rega, G. A. Petersson, H. Nakatsuji, M. Hada, M. Ehara, K. Toyota, R. Fukuda, J. Hasegawa, M. Ishida, T. Nakajima, Y. Honda, O. Kitao, H. Nakai, M. Klene, X. Li, J. E. Knox, H. P. Hratchian, J. B. Cross, V. Bakken, C. Adamo, J. Jaramillo, R. Gomperts, R. E. Stratmann, O. Yazyev, A. J. Austin, R. Cammi, C. Pomelli, J. W. Ochterski, P. Y. Ayala, K. Morokuma, G. A. Voth, P. Salvador, J. J. Dannenberg, V. G. Zakrzewski, S. Dapprich, A. D. Daniels, M. C. Strain, O. Farkas, D. K. Malick, A. D. Rabuck, K. Raghavachari, J. B. Foresman, J. V. Ortiz, Q. Cui, A. G. Baboul, S. Clifford, J. Cioslowski, B. B. Stefanov, G. Liu, A. Liashenko, P. Piskorz, I. Komaromi, R. L. Martin, D. J. Fox, T. Keith, M. A. Al-Laham, C. Y. Peng, A. Nanayakkara, M. Challacombe, P. M. W. Gill, B. Johnson, W. Chen, M. W. Wong, C. Gonzalez, and J. A. Pople. Gaussian 03, Revision C.02, 2003. Gaussian, Inc., Wallingford, CT, 2004.
- [23] L. A. Girifalco and R. A. Lad. Energy of cohesion, compressibility, and the potential energy functions of the graphite system. *The Journal of Chemical Physics*, 25(4): 693–697, 1956. doi:10.1063/1.1743030.
- [24] C. G. Gray and K. E. Gubbins. *Theory of Molecular Fluids: Fundamentals*. Oxford University Press, Oxford, 1984.
- [25] W. J. Grieco, A. L. Lafleur, K. C. Swallow, H. Richter, K. Taghizadeh, and J. B. Howard. Fullerenes and PAH in low-pressure premixed benzene/oxygen flames. *Symposium (International) on Combustion*, 27(2):1669–1675, 1998. doi:10.1016/S0082-0784(98)80006-4.
- [26] S. Grimme and C. Mück-Lichtenfeld. Noncovalent interactions between graphene sheets and in multishell (hyper)fullerenes. *The Journal of Physical Chemistry C*, 111:11199–11207, 2007. doi:10.1021/jp0720791.
- [27] J. Happold, H. Grotheer, and M. Aigner. Distinction of gaseous soot precursor molecules and soot precursor particles through photoionization mass spectrometry. *Rapid Communications in Mass Spectrometry*, 21(7):1247–1254, 2007. doi:10.1002/rcm.2955.
- [28] J. D. Herdman and J. H. Miller. Intermolecular potential calculations for polynuclear aromatic hydrocarbon clusters. *Journal of Physical Chemistry A*, 112(28):6249–6256, 2008. doi:10.1021/jp800483h.
- [29] A. Heßelmann and G. Jansen. First-order intermolecular interaction energies from Kohn-Sham orbitals. *Chemical Physics Letters*, 357(5-6):464–470, 2002. doi:10.1016/S0009-2614(02)00538-9.
- [30] A. Heßelmann and G. Jansen. Intermolecular induction and exchange-induction energies from coupled-perturbed Kohn-Sham density functional theory. *Chemical Physics Letters*, 362(3-4):319–325, 2002. doi:10.1016/S0009-2614(02)01097-7.

- [31] A. Heßelmann and G. Jansen. Intermolecular dispersion energies from time-dependent density functional theory. *Chemical Physics Letters*, 367(5-6):778–784, 2003. doi:10.1016/S0009-2614(02)01796-7.
- [32] A. Heßelmann, G. Jansen, and M. Schütz. Density-functional theory-symmetry-adapted intermolecular perturbation theory with density fitting: A new efficient method to study intermolecular interaction energies. *The Journal of Chemical Physics*, 122(1):014103, 2005. doi:10.1063/1.1824898.
- [33] M. P. Hodges, R. J. Wheatley, G. K. Schenter, and A. H. Harvey. Intermolecular potential and second virial coefficient of the water–hydrogen complex. *The Journal of Chemical Physics*, 120(2):710–720, 2004. doi:10.1063/1.1630960.
- [34] T. Ishiguro, Y. Takatori, and K. Akihama. Microstructure of Diesel Soot Particles Probed by Electron Microscopy: First Observation of Inner Core and Outer Shell. *Combustion and Flame*, 108(1-2):231–234, 1997. doi:10.1016/S0010-2180(96)00206-4.
- [35] W. L. Jorgensen and D. L. Severance. Aromatic-aromatic interactions: free energy profiles for the benzene dimer in water, chloroform, and liquid benzene. *Journal of the American Chemical Society*, 112(12):4768–4774, 1990. doi:10.1021/ja00168a022.
- [36] W. L. Jorgensen, J. D. Madura, and C. J. Swenson. Optimized intermolecular potential functions for liquid hydrocarbons. *Journal of the American Chemical Society*, 106(22):6638–6646, 1984. doi:10.1021/ja00334a030.
- [37] G. Karlström, P. Linse, A. Wallqvist, and B. Joansson. Intermolecular potentials for the water-benzene and the benzene-benzene systems calculated in an ab initio SCFCI approximation. *Journal of the American Chemical Society*, 105(12):3777–3782, 1983. doi:10.1021/ja00350a004.
- [38] R. A. Kendall, T. H. Dunning, Jr., and R. J. Harrison. Electron affinities of the first-row atoms revisited. Systematic basis sets and wave functions. *The Journal of Chemical Physics*, 96(9):6796–6806, 1992. doi:10.1063/1.462569.
- [39] D. C. Langreth, M. Dion, H. Rydberg, E. Schröder, P. Hyldgaard, and B. I. Lundqvist. Van der waals density functional theory with applications. *International Journal of Quantum Chemistry*, 101(5):599–610, 2005. doi:10.1002/qua.20315.
- [40] S. Lebègue, J. Harl, T. Gould, J. G. Ángyán, G. Kresse, and J. F. Dobson. Cohesive properties and asymptotics of the dispersion interaction in graphite by the random phase approximation. *Physics Review Letters*, 105(19):196401, 2010. doi:10.1103/PhysRevLett.105.196401.
- [41] Z. Li and H. A. Scheraga. Monte carlo-minimization approach to the multiple-minima problem in protein folding. *Proceedings of the National Academy of Sciences of the United States of America*, 84(19):6611–6615, 1987.

- [42] J. P. M. Lommerse, W. D. S. Motherwell, H. L. Ammon, J. D. Dunitz, A. Gavezzotti, D. W. M. Hofmann, F. J. J. Leusen, W. T. M. Mooij, S. L. Price, B. Schweizer, M. U. Schmidt, B. P. van Eijck, P. Verwer, and D. E. Williams. A test of crystal structure prediction of small organic molecules. *Acta Crystallographica Section B*, 56(4): 697–714, 2000. doi:10.1107/S0108768100004584.
- [43] Z. Lui, J. Lui, Y. Cheng, and Q. Zheng. Interlayer binding energy of graphite – a direct experimental determination, 2011. arXiv:1104.1469v1 [cond-mat.mes-hall].
- [44] E. M. Mas, K. Szalewicz, R. Bukowski, and B. Jeziorski. Pair potential for water from symmetry-adapted perturbation theory. *The Journal of Chemical Physics*, 107(11):4207–4218, 1997. doi:10.1063/1.474795.
- [45] A. J. Misquitta and A. J. Stone. Distributed polarizabilities obtained using a constrained density-fitting algorithm. *The Journal of Chemical Physics*, 124(2):024111, 2006. doi:10.1063/1.2150828.
- [46] A. J. Misquitta and A. J. Stone. Dispersion energies for small organic molecules: first row atoms. *Molecular Physics*, 106(12-13):1631–1643, 2008. doi:10.1080/00268970802258617.
- [47] A. J. Misquitta and A. J. Stone. Accurate induction energies for small organic molecules: 1. Theory. *Journal of Chemical Theory and Computation*, 4(1):7–18, 2008. doi:10.1021/ct700104t.
- [48] A. J. Misquitta and K. Szalewicz. Intermolecular forces from asymptotically corrected density functional description of monomers. *Chemical Physics Letters*, 357(3-4):301–306, 2002. doi:10.1016/S0009-2614(02)00533-X.
- [49] A. J. Misquitta and K. Szalewicz. Symmetry-adapted perturbation-theory calculations of intermolecular forces employing density-functional description of monomers. *The Journal of Chemical Physics*, 122(21):214109, 2005. doi:10.1063/1.1924593.
- [50] A. J. Misquitta, B. Jeziorski, and K. Szalewicz. Dispersion energy from density-functional theory description of monomers. *Phys. Rev. Lett.*, 91(3):033201, 2003. doi:10.1103/PhysRevLett.91.033201.
- [51] A. J. Misquitta, R. Podeszwa, B. Jeziorski, and K. Szalewicz. Intermolecular potentials based on symmetry-adapted perturbation theory with dispersion energies from time-dependent density-functional calculations. *The Journal of Chemical Physics*, 123(21):214103, 2005. doi:10.1063/1.2135288.
- [52] A. J. Misquitta, A. J. Stone, and S. L. Price. Accurate induction energies for small organic molecules. 2. Development and testing of distributed polarizability models against SAPT(DFT) energies. *Journal of Chemical Theory and Computation*, 4(1): 19–32, 2008. doi:10.1021/ct700105f.
- [53] A. J. Misquitta, G. W. A. Welch, A. J. Stone, and S. L. Price. A first principles prediction of the crystal structure of C₆BrClFH₂. *Chemical Physics Letters*, 456(1-3):105–109, 2008. doi:10.1016/j.cplett.2008.02.113.

- [54] A. J. Misquitta, J. Spencer, A. J. Stone, and A. Alavi. Dispersion interactions between semiconducting wires. *Phys. Rev. B*, 82(7):075312, 2010. doi:10.1103/PhysRevB.82.075312.
- [55] J. B. O. Mitchell, S. L. Price, M. Leslie, D. Buttar, and R. J. Roberts. Anisotropic repulsion potentials for cyanuric chloride ($C_3N_3Cl_3$) and their application to modeling the crystal structures of azaaromatic chlorides. *The Journal of Physical Chemistry A*, 105(43):9961–9971, 2001. doi:10.1021/jp0125350.
- [56] S. Mosbach, M. S. Celnik, A. Raj, M. Kraft, H. R. Zhang, S. Kubo, and K. Kim. Towards a detailed soot model for internal combustion engines. *Combustion and Flame*, 156(6):1156–1165, 2009. doi:10.1016/j.combustflame.2009.01.003.
- [57] J. P. Perdew, K. Burke, and M. Ernzerhof. Generalized gradient approximation made simple. *Physical Review Letters*, 77(18):3865–3868, 1996. doi:10.1103/PhysRevLett.77.3865.
- [58] J. Pillardy, Y. A. Arnautova, C. Czaplowski, K. D. Gibson, and H. A. Scheraga. Conformation-family monte carlo: A new method for crystal structure prediction. *Proceedings of the National Academy of Sciences of the United States of America*, 98(22):12351–12356, 2001. doi:10.1073/pnas.231479298.
- [59] R. Podeszwa. Interactions of graphene sheets deduced from properties of polycyclic aromatic hydrocarbons. *The Journal of Chemical Physics*, 132(4):044704, 2010. doi:10.1063/1.3300064.
- [60] R. Podeszwa and K. Szalewicz. Physical origins of interactions in dimers of polycyclic aromatic hydrocarbons. *Physical Chemistry Chemical Physics*, 10(19):2735–2746, 2008. doi:10.1039/b719725j.
- [61] R. Podeszwa, R. Bukowski, and K. Szalewicz. Potential energy surface for the benzene dimer and perturbational analysis of π - π interactions. *The Journal of Physical Chemistry A*, 110(34):10345–10354, 2006. doi:10.1021/jp064095o.
- [62] S. L. Price and L. S. Price. Modelling intermolecular forces for organic crystal structure prediction. In D. Mingos and D. J. Wales, editors, *Intermolecular Forces and Clusters I: Structure and Bonding*, volume 115, pages 81–123. Springer-Verlag, Berlin Heidelberg, 2nd edition, 2005.
- [63] S. L. Price, M. Leslie, G. W. A. Welch, M. Habgood, L. S. Price, P. G. Karamertzanis, and G. M. Day. Modelling organic crystal structures using distributed multipole and polarizability-based model intermolecular potentials. *Physical Chemistry Chemical Physics*, 12(30):8478–8490, 2010. doi:10.1039/c004164e.
- [64] A. Raj, P. L. W. Man, T. S. Totton, M. Sander, R. Shirley, M. S. Celnik, and M. Kraft. New pah processes to improve the model prediction of the composition of combustion-generated pahs and soot. *Carbon*, 48.

- [65] A. Raj, M. S. Celnik, R. Shirley, M. Sander, R. I. A. Patterson, R. H. West, and M. Kraft. A statistical approach to develop a detailed soot growth model using PAH characteristics. *Combustion and Flame*, 156(4):896–913, 2009. doi:10.1016/j.combustflame.2009.01.005.
- [66] A. Raj, M. Sander, V. Janardhanan, and M. Kraft. A study on the coagulation of polycyclic aromatic hydrocarbon clusters to determine their collision efficiency. *Combustion and Flame*, 157(3):523–534, 2010. doi:10.1016/j.combustflame.2009.10.003.
- [67] M. Rapacioli, F. Calvo, F. Spiegelman, C. Joblin, and D. J. Wales. Stacked clusters of polycyclic aromatic hydrocarbon molecules. *Journal of Physical Chemistry A*, 109(11):2487–2497, 2005. doi:10.1021/jp046745z.
- [68] M. Rubeš and O. Bludský. Intermolecular π - π interactions in solids. *Physical Chemistry Chemical Physics*, 10(19):2611–2615, 2008. doi:10.1039/B718701G.
- [69] U. C. Singh and P. A. Kollman. An approach to computing electrostatic charges for molecules. *Journal of Computational Chemistry*, 5(2):129–145, 1984. doi:10.1002/jcc.540050204.
- [70] L. Spanu, S. Sorella, and G. Galli. Nature and strength of inter-layer binding in graphite. *Physics Review Letters*, 103(19):196401, 2009. doi:10.1103/PhysRevLett.103.196401.
- [71] T. L. Starr and D. E. Williams. Comparison of models for h_2 - h_2 and h_2 - he anisotropic intermolecular repulsion. *The Journal of Chemical Physics*, 66(5):2054–2057, 1977. doi:10.1063/1.434165.
- [72] A. J. Stone. Distributed multipole analysis: Stability for large basis sets. *Journal of Chemical Theory and Computation*, 1(6):1128–1132, 2005. doi:10.1021/ct050190+.
- [73] A. J. Stone. GDMA: a program for performing Distributed Multipole Analysis of wavefunctions calculated using the Gaussian program system, 2009. <http://www-stone.ch.cam.ac.uk/programs.html>.
- [74] A. J. Stone, A. Dullweber, O. Engkvist, E. Frascini, M. P. Hodges, A. W. Meredith, D. R. Nutt, P. L. A. Popelier, and D. J. Wales. ORIENT: a program for studying interactions between molecules, version 4.6, University of Cambridge, 2002. <http://www-stone.ch.cam.ac.uk/programs.html>.
- [75] H. Takeuchi. Novel method for geometry optimization of molecular clusters: Application to benzene clusters. *Journal of Chemical Information and Modeling*, 47(1):104–109, 2007. doi:10.1021/ci600336p.
- [76] K. T. Tang and J. P. Toennies. An improved simple model for the van der waals potential based on universal damping functions for the dispersion coefficients. *The Journal of Chemical Physics*, 80(8):3726–3741, 1984. doi:10.1063/1.447150.
- [77] T. S. Totton, D. Chakrabarti, A. J. Misquitta, D. J. Wales, and M. Kraft. Modelling the internal structure of nascent soot particles. *Combustion and Flame*, 157(5):909–914, 2010. doi:10.1016/j.combustflame.2009.11.013.

- [78] T. S. Totton, A. J. Misquitta, and M. Kraft. A first principles development of a general anisotropic potential for polycyclic aromatic hydrocarbons. *Journal of Chemical Theory and Computation*, 6(3):683–695, 2010. doi:10.1021/ct9004883.
- [79] T. S. Totton, A. J. Misquitta, and M. Kraft. A transferable electrostatic model for intermolecular interactions between polycyclic aromatic hydrocarbons. *Chemical Physics Letters*, 510(1-3):154–160, 2011. doi:10.1016/j.cplett.2011.05.021.
- [80] M. Tremayne, L. Grice, J. C. Pyatt, C. C. Seaton, B. M. Kariuki, H. H. Y. Tsui, S. L. Price, and J. C. Cherryman. Characterization of complicated new polymorphs of chlorothalonil by x-ray diffraction and computer crystal structure prediction. *Journal of the American Chemical Society*, 126(22):7071–7081, 2004. doi:10.1021/ja0498235.
- [81] B. W. van de Waal. Calculated ground-state structures of 13-molecule clusters of carbon dioxide, methane, benzene, cyclohexane, and naphthalene. *Journal of Chemical Physics*, 79(8):3948–3961, 1983. doi:10.1063/1.446263.
- [82] R. L. Vander Wal, A. Yezerets, N. W. Currier, D. H. Kim, and C. M. Wang. HRTEM Study of diesel soot collected from diesel particulate filters. *Carbon*, 45:70–77, 2007. doi:10.1016/j.carbon.2006.08.005.
- [83] D. J. Wales and T. V. Bogdan. GMIN: a program for finding global minima and calculating thermodynamic properties from basinsampling, 2009. <http://www-wales.ch.cam.ac.uk/GMIN>.
- [84] D. J. Wales and J. P. K. Doye. Global optimization by basin-hopping and the lowest energy structures of Lennard-Jones clusters containing up to 110 atoms. *The Journal of Physical Chemistry A*, 101(28):5111–5116, 1997. doi:10.1021/jp970984n.
- [85] P. Weilmünster, A. Keller, and K. H. Homann. Large Molecules, Radicals, Ions, and Small Soot Particles in Fuel-Rich Hydrocarbon Flames Part I: Positive Ions of Polycyclic Aromatic Hydrocarbons (PAH) in Low-Pressure Premixed Flames of Acetylene and Oxygen. *Combustion and Flame*, 116:62–83, 1999. doi:10.1016/S0010-2180(98)00049-2.
- [86] D. E. Williams. Nonbonded potential parameters derived from crystalline hydrocarbons. *The Journal of Chemical Physics*, 47(11):4680–4684, 1967. doi:10.1063/1.1701684.
- [87] D. E. Williams. Improved intermolecular force field for crystalline hydrocarbons containing four- or three-coordinated carbon. *Journal of Molecular Structure*, 485-486:321–347, 1999. doi:10.1016/S0022-2860(99)00092-7.
- [88] D. E. Williams. Improved intermolecular force field for crystalline oxohydrocarbons including O–H...O hydrogen bonding. *Journal of Computational Chemistry*, 22(1): 1–20, 2001. doi:10.1002/1096-987X(20010115)22:1::AID-JCC2;3.0.CO;2-6.
- [89] D. E. Williams. Improved intermolecular force field for molecules containing H, C, N, and O atoms, with application to nucleoside and peptide crystals. *Journal of Computational Chemistry*, 22(11):1154–1166, 2001. doi:10.1002/jcc.1074.

- [90] D. E. Williams and T. L. Starr. Calculation of the crystal structures of hydrocarbons by molecular packing analysis. *Computers and Chemistry*, 1(3):173–177, 1977. doi:10.1016/0097-8485(77)85007-9.
- [91] G. J. Williams and A. J. Stone. Distributed dispersion: A new approach. *The Journal of Chemical Physics*, 119(9):4620–4628, 2003. doi:10.1063/1.1594722.
- [92] D. Wong, R. Whitesides, C. A. Schuetz, and M. Frenklach. Soot precursors consisting of stacked pericondensed pahs. In H. Bockhorn, A. D’Anna, A. F. Sarofim, and H. Wang, editors, *Combustion Generated Fine Carbonaceous Particles*, pages 275–285. Karlsruhe University Press, 2007.
- [93] C. J. Wormald, E. J. Lewis, and A. J. Terry. Second virial coefficients of benzene and cyclohexane from measurements of the excess molar enthalpy of $(0.5\text{N}_2 + 0.5\text{C}_6\text{H}_6)$ and $(0.5\text{N}_2 + 0.5\text{C}_6\text{H}_{12})$ from 333.2 k to 433.2 k. *The Journal of Chemical Thermodynamics*, 28(1):17–27, 1996. doi:10.1006/jcht.1996.0004.
- [94] R. Zacharia, H. Ulbricht, and T. Hertel. Interlayer cohesive energy of graphite from thermal desorption of polyaromatic hydrocarbons. *Physical Review B*, 69(15):155406, 2004. doi:10.1103/PhysRevB.69.155406.
- [95] T. Zykova-Timan, P. Raiteri, and M. Parrinello. Investigating the polymorphism in PR179: A combined crystal structure prediction and metadynamics study. *The Journal of Physical Chemistry B*, 112(42):13231–13237, 2008. doi:10.1021/jp802977t.